NRC Research Press

ARTICLE

Chemotyping using synchrotron mid-infrared and X-ray spectroscopy to improve agricultural production[1]

K. Tanino, I.R. Willick, K. Hamilton, P. Vijayan, Y. Jiang, G.S. Brar, P. Yu, L. Kalcsits, R. Lahlali, B. Smith, D. Brian Fowler, R. Kutcher, R. Bueckert, T. Warkentin, and C. Karunakaran

Abstract: Synchrotron techniques are powerful tools in material and environmental sciences; however, they are currently underutilized in plant research. The Canadian Light Source synchrotron at the University of Saskatchewan campus is the only such facility in Canada open to academic, government, and industrial clients. This review introduces the potential of synchrotron-based spectroscopic methods and its applications to agriculture and plant sciences. Relative ease of sample preparation, nondestructive analysis, high spatial resolution, and multiple response measurements within a single sample are among its advantages. Synchrotron-based Fourier transform mid-infrared spectromicroscopy, X-ray absorption, and fluorescence spectromicroscopy are included in the several approaches discussed. Examples range from evaluating protein secondary structure and nondestructive compositional analysis of leaf epicuticular wax and pollen surface lipids to cell wall composition and nutrient analyses. Synchrotron technology can help to initially identify key spectra related to plant properties for subsequent higher throughput techniques. One example is the adaptation of synchrotron techniques for lower resolution analysis in the field such as nondestructive elemental analysis for localization of nutrients in fruit crops using handheld high-throughput devices. In addition, interest in creating high-throughput systems based on synchrotron technology itself is driving the development of new hardware to meet these larger challenges.

Key words: agriculture, X-ray, horticulture, infrared, lipids, nutrients, protein, synchrotron.

Résumé : Le synchrotron est un outil puissant couramment employé dans la science des matériaux et les sciences de l'environnement. Malheureusement, ses techniques sont souvent mal exploitées dans la recherche sur les plantes. Le Centre canadien de rayonnement synchrotron de l'Université de la Saskatchewan est la seule installation du genre au Canada. Peut y recourir sa clientèle du milieu universitaire, du gouvernement et de l'industrie. L'article que voici donne un aperçu des possibilités que présentent les méthodes spectroscopiques articulées sur le synchrotron et leur application à l'agriculture ainsi qu'aux sciences végétales. La facilité relative avec laquelle les échantillons sont préparés, l'analyse non destructive, la forte résolution spatiale et les nombreuses réactions jaugées grâce au même échantillon en sont quelques avantages. La spectromicroscopie à transformée de Fourier dans le mi-infrarouge, la spectromicroscopie par absorption des rayons X et la spectromicroscopie à fluorescence qu'autorise le synchrotron font partie des approches examinées. On peut notamment s'en servir pour évaluer la structure secondaire des protéines, pour analyser de façon non destructive la composition de la cire épicuticulaire des feuilles ou celle des lipides à la surface du pollen, voire pour analyser la paroi cellulaire et les éléments nutritifs. La technologie du synchrotron facilite l'identification des principales raies spectrales

Received 18 November 2016. Accepted 11 July 2017.

K. Tanino, I.R. Willick, K. Hamilton, P. Vijayan, Y. Jiang, B. Smith, D.B. Fowler, and R. Bueckert. Department of Plant Sciences, College of Agriculture and Bioresources, University of Saskatchewan, Saskatoon, SK S7N 5A8, Canada.

G.S. Brar, R. Kutcher, and T. Warkentin. Department of Plant Sciences, College of Agriculture and Bioresources, University of Saskatchewan, Saskatoon, SK S7N 5A8, Canada; Crop Development Centre, College of Agriculture and Bioresources, University of Saskatchewan, Saskatoon, SK S7N 5A8, Canada.

P. Yu. Department of Animal and Poultry Science, College of Agriculture and Bioresources, University of Saskatchewan, Saskatoon, SK S7N 5A8, Canada.

L. Kalcsits. Department of Horticulture, Washington State University, WSU Tree Fruit Research and Extension Center, 1100 North Western Avenue, Wenatchee, WA 98801 USA.

R. Lahlali and C. Karunakaran. Canadian Light Source, 44 Innovation Boulevard, Saskatoon SK S7N 2V3, Canada.

Corresponding author: Karen Tanino (email: karen.tanino@usask.ca).

[1]This paper is part of a Special Issue entitled "2016 Joint Meeting of the Canadian Society of Agronomy and the Canadian Society of Horticultural Science, 24–26 July 2016, Montreal, QC".

associées aux propriétés des végétaux avant leur analyse avec des techniques à débit plus élevé. L'adaptation des techniques du synchrotron à l'analyse à faible résolution sur le terrain, pour déterminer de manière non destructive la composition des fruits et y situer les éléments nutritifs avec un appareil manuel à débit élevé, en est un exemple. L'intérêt que suscitent les systèmes à débit élevé s'appuyant sur la technologie du synchrotron est propice au développement de nouveaux appareils capables de relever de plus grands défis. [Traduit par la Rédaction]

Mots-clés : agriculture, rayons X, horticulture, infrarouge, lipides, oligoéléments, protéines, synchrotron.

Introduction

Selecting environmental stress resistance traits with improvements in crop yield and quality requires the consideration of a multitude of factors (Buddenhagen 1983; Fiorani and Schurr 2013; Walter et al. 2015). Advancements in molecular and analytical techniques have broadened the concept of quantitative analysis to include the characterization of biological processes, functions, and anatomical structures (reviewed by Fiorani and Schurr 2013; Walter et al. 2015). This has led to an increased demand for high-throughput phenotyping methods that can measure these traits in tens of thousands of plant samples within the short time intervals available between harvesting and subsequent planting. Only then can these traits be used by breeders to select and advance superior breeding lines to the next generation. Development of X-ray and mid-infrared (MIR) spectroscopy-based phenotyping techniques using synchrotron beamlines have the potential of enabling high-throughput phenotyping of many such traits.

In the last 15 yr, phenotyping has been linked to nondestructive optical analyses of plant traits based on imaging (Zhao et al. 2014; Vijayan et al. 2015; Walter et al. 2015). Synchrotron-based technology affords researchers the ability to image and quantify specific chemicals or functional groups as well as nutrients within important plant tissues (Vijayan et al. 2015). This has enabled researchers to examine anatomic and biochemical responses, making it a potential for phenotyping or chemotyping specific traits of interest (Jiang et al. 2015; Lahlali et al. 2014, 2015, 2016*a*; Kalcsits 2016; Willick et al. 2017). Different synchrotron techniques have been applied to the identification of desirable genotypes, such as heat tolerance traits in field pea (*Pisum sativum* L.) pollen (Lahlali et al. 2014; Jiang et al. 2015), drought tolerance traits in spring wheat (*Triticum aestivum* L.), and biochemical and anatomical traits associated with enhanced tolerance to *Fusarium* head blight (FHB) caused by *Fusarium graminearum* Schwabe in wheat (Lahlali et al. 2015, 2016*a*) or used as a tool to select for enhanced micronutrient composition in apple (*Malus domestica* Borkh.) and pear (*Pyrus communis*) cultivars (Kalcsits 2016).

The Canadian Light Source (CLS) synchrotron is the largest science project of its time in Canada and is situated on the University of Saskatchewan campus. The CLS is the only synchrotron in Canada and has operating beamlines for energy levels ranging from far-infrared through to soft and hard X-rays. A competitive application system evaluates user proposals through an international review panel. Approved proposals enable academic and government researchers to gain access to the facility. As the focus of plant phenotyping has broadened from basic science to more applied research, synchrotron-based technologies have additional information to offer to enhance plant breeding efforts.

Synchrotron Techniques Used in Plant Chemotyping

The dissection of a specific cell or tissue of interest at a particular developmental stage in a crop's lifecycle is seldom practiced and traditional analysis using gas or liquid chromatography requires large amounts of dried tissue (in the microgram to milligram scale). Analysis of small samples such as pollen (Jiang et al. 2015) or delicate tissues such as the nodes of a wheat rachis (Lahlali et al. 2015, 2016*a*, 2016*b*) requires harvesting hundreds of plants to accrue enough tissue for analyses. Traditional bulk chemical analyses can average out the intrinsic heterogeneity of certain plant tissues, potentially masking phenotypes (McCann et al. 1997). The use of Fourier transform infrared (FTIR) spectroscopy and X-ray absorption spectroscopy in conjunction with microscopy or equipment adapted for handheld field use will facilitate the identification of novel traits. The objective of this paper is to highlight synchrotron applications that can be used in agriculture and plant science research. The case studies in this article are not exhaustive but provide research examples of the value of using these approaches. This review will focus on two spectroscopy techniques commonly employed at the CLS for plant science research: MIR and X-ray absorption spectroscopy.

Mid-infrared spectroscopy

The MIR region (4000–200 wavenumbers, measured in cm^{-1}) of the electromagnetic spectrum corresponds to molecular vibrations associated with chemical bonds in organic compounds. Using these vibrational signatures, we can identify specific peaks associated with organic compounds such as cellulose, protein, or lignin. Mid-infrared light can be used to identify and quantify the distribution of these chemical components within intact plant tissues, homogenized bulk tissues, or tissue sections. When coupled with the appropriate detector or microscope, FTIR can image a region of interest as small as 2 μm, allowing for the identification of differences in cell

wall composition (McCann et al. 1997; Tanino et al. 2013; Vijayan et al. 2015). Implementation of recent advances in techniques like near-field scanning optical microscopy and atomic force microscopy have enabled nano-FTIR instruments with a spatial resolution of up to 20 nm (Huth et al. 2012).

Conventional infrared spectromicroscopes are equipped with globar sources (silicon carbide) and have large beams sufficient for characterization of bulk samples or large samples with low spatial resolution (15 μm). These microscopes are used for fast screening of multiple samples. Synchrotron light provides 1000 times more infrared light than globar sources in a small focussed area. Therefore, synchrotron-based infrared spectromicroscopes are used to acquire high spatial resolution data in a short time with high signal to noise ratio.

The CLS MIR beamline has two microscopes. The globar source based spectromicroscope (IFS 66 V/S, Bruker Optics, Ettlingen, Germany) is often used for bulk spectroscopy, sample surface characterization [attenuated total internal reflection (ATR) spectroscopy], and low-resolution spectromicroscopy. For bulk spectroscopy, harvested tissue samples are frozen in liquid nitrogen and then freeze dried. Approximately 2 mg of freeze dried sample is ground finely with 98 mg of KBr powder and made into a pellet (Lahlali et al. 2015). The spectrum of each sample (average of 64–256 or 512 scans depending on the sample absorption) is then normalized using the spectrum of pure KBr pellet (average of 128 or 256 scans). For surface characterization, fresh samples such as leaves (Fig. 1) or small samples such as pollen can be placed on CaF_2 windows for data collection (Jiang et al. 2015). Two types of ATR probes (probe area 3 mm or 200 μm) are available for use with large or small samples, respectively. The spectromicroscope has a deuterated triglycine sulphate detector for bulk spectroscopy and a mercury cadmium telluride detector for low resolution spectromicroscopy of thin sectioned (~10 μm) samples in transmission mode.

The synchrotron-based spectromicroscope (Vertex 70v Interferometer with a Hyperion 3000 infrared microscope, Bruker Optics) has mercury cadmium telluride and focal plane array (FPA) detectors. These detectors are used for low and high spatial resolution spectromicroscopy data collection, respectively. All data collection (4000–800 cm^{-1} at 2 or 4 cm^{-1} resolution) and initial data analysis in the MIR beamline are conducted using OPUS software (version 7.0, Bruker Optics Inc., Billerica, MA).

X-ray absorption spectroscopy

Essential macro- and micro-nutrients are present in different concentrations in plants. Laboratory-based X-ray sources can be used to determine the presence of high concentrations of nutrients. However, synchrotron sources are normally acquired (ppm to ppb) to determine the presence of low concentrated nutrients due to the source brightness and the form of nutrients

Fig. 1. The IFS 66 V/S Bruker FTIR with an ATR attachment at the CLS Mid-Infrared 01B1-1 Beamline. An ATR accessory measures changes that occur in an internally reflected infrared beam (3) when the beam comes in contact with a sample (2). Samples are held in place by a pressure tower (1). In regions of the infrared spectrum where the corn sample absorbs energy, the light will be attenuated. The attenuated beam returns to the crystal and is directed to a detector in the infrared spectrometer. Here the attenuated infrared beam is recorded as an interferogram signal that can be used to generate an infrared spectrum. [Colour online.]

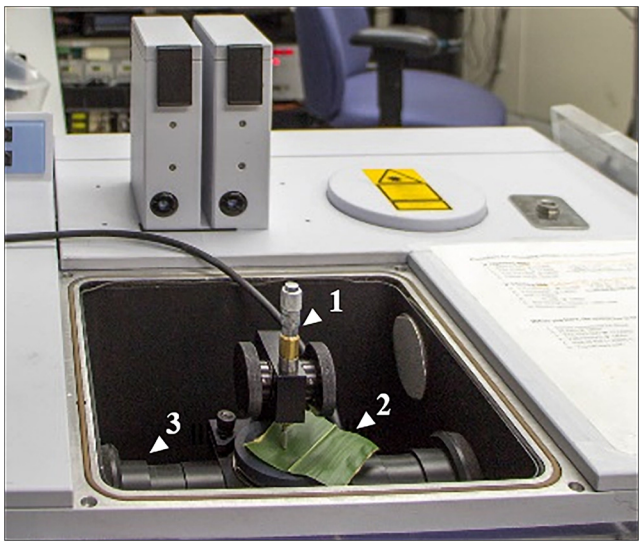

(e.g., iron phosphate as opposed to iron sulphate; Fe^{2+} or Fe^{3+}) due to high X-ray energy sensitivity (Vijayan et al. 2015). Furthermore, the presence of nutrients such as S, P, Ca, K, Mg, Fe, Zn, and Se can be determined simultaneously in bulk samples or can be mapped for spatial localization studies in thin sample sections on a micrometre to nanometre scale using synchrotron sources.

The CLS has several soft and hard X-ray beamlines that can be used for plant samples. Soft X-ray beamlines have high sensitivity for low atomic weight elements such as C, N, O, S, P, Ca, and K, while hard X-ray beamlines have high sensitivity for heavy elements such as Mg, Fe, Cu, Zn, and Se. Sample sections should be thin (approximately 10 μm) if tissue nutrient concentrations are high and data are collected in the transmission mode. However, sample thickness does not matter in the fluorescence mode of samples with low concentrations of elements of interest. The X-ray fluorescence (XRF) spectra of most samples reported in this review were collected at the Industry Development Education and Applications for Students beamline at the CLS. A Ge (220) crystal in the monochromator and a 13 element Canberra Ge detector were used to record the partial XRF. The energy of the incident X-ray beam was 12.8 keV and the detector in the fluorescence mode was used to record sample spectra (1.2–20 keV).

Applications of Synchrotron Technology

The following are specific examples in plant agriculture covering a range of response measurements based on a few of the beamlines at the CLS. These examples have been selected to provide an overview of how this powerful technology can be utilized.

Leaf epicuticular wax as markers for low temperature responses in corn

Corn [*Zea mays* (L.) subsp. Mays] is the most widely produced crop worldwide based on tonnage and is used for food, feed, and fuel (Food and Agriculture Organization of the United Nations 2013). While corn is generally chilling-sensitive, variation of this trait reveals chilling-resistant types (data not shown). All corn, however, is frost-sensitive. With the projected increase in yield losses caused by frost over the growing season (Gu et al. 2008) and the industry-led investment to expand corn acreage into northern latitudes (Monsanto Canada 2013; Dupont Pioneer 2017), a greater emphasis needs to be placed on identifying new traits in corn frost avoidance. Leaf epicuticular wax is an important barrier to frost that can mitigate the external nucleation of ice on plant tissues (Wisniewski and Fuller 1999; Bird and Gray 2003). The MIR beamline at the CLS generates specific wavelengths of brilliant synchrotron light optimized for analyzing large biomolecules, such as epicuticular wax (CH_2 groups).

Leaf epicuticular wax composition has been studied in corn grown under warm and chilling conditions (Vigh et al. 1981) but the influence of chilling temperatures on subsequent frost injury has not been previously examined. In this preliminary test, four corn genotypes were grown in a controlled environment greenhouse on a 28 °C day and 22 °C night cycle under a 16 h photoperiod. Vegetative leaves five, six and seven from mature corn plants were sampled during the early reproductive stage. Chilling conditions of 18 °C day and 6 °C night cycles under a 12 h photoperiod represented the 30-yr average for the 10 d prior to the first fall frost. Leaf samples under the greenhouse and chilling treatments were evaluated through nondestructive leaf cuticular surface assessment using ATR. The adaxial surface of mature leaves were measured with a 3 mm ATR probe (Fig. 1). Leaf samples secured in the ATR probe accessory were collected in the reflectance spectra collection mode with an average of 512 scans. All spectra resultant from ATR-FTIR measurements have extended ATR correction and were normalized to the amide II peak (1600–1700 cm^{-1}), then analyzed before and after the second derivative for peak identification in the lipid region. The second derivative was utilized to localize the accentuated definition of the peak regions of interest (Fig. 2B). Peak area integration was performed across the CH_2 groups. Three areas of interest were identified: asymmetrical CH_2, symmetrical CH_2, and combined CH_2 groups (Fig. 2A). Chilling-treated samples have a lower peak

Fig. 2. (A) Lipid fingerprint region 2800–3000 cm^{-1} of corn epicuticular wax leaf spectra from an average of two samples of each of three biological replications. Spectra were taken from plants that were grown under nonchilling and chilling conditions. (B) Second-derivative spectra isolating asymmetrical and symmetrical CH_2 peaks (K. Hamilton et al., unpublished data).

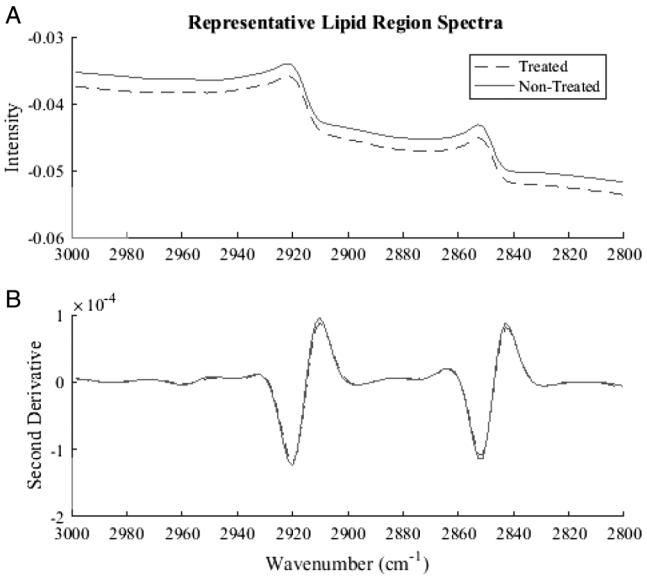

intensity, indicating the prevalence of lipids has decreased following chilling pretreatment. Mid-infrared light can be optimized to measure lipids of cuticular waxes on leaf surfaces and differences between chilling treatments (K. Hamilton et al., unpublished data). The quantity, measured through CH_2 peak intensity, was reduced through chilling treatment and the peak identification was performed using the second derivative (Figs. 2A, 2B). This methodology is efficient and offers high throughput for evaluating multiple genotypes across treatments (Leugers et al. 2003; Kazarian and Chan 2010).

Lipid and protein composition of pollen as markers for heat tolerance in pea

The plant pollen surface consists of a coat and exine layer comprised of lipids and proteins that affect pollen hydration and germination success (Dickinson1993; Wolters-Arts et al. 1998). Quantifying pollen surface lipids through conventional methods (such as mass spectroscopy) is challenging because samples are small, expensive to collect, and separating the coat and exine from the rest of pollen is time consuming. Synchrotron tools are advantageous because they can spatially resolve small biological tissue samples, including their chemical composition, particularly in samples where precisely isolating cell layers in tissues and within cells is difficult, if not impossible, through conventional methods. Synchrotron FTIR requires only minimal sample preparation, is rapid and noninvasive, and provides information on protein, lipid, and carbohydrate composition

(Martín et al. 2005), but is under utilized in plant science research.

The objective of the Jiang et al. (2015) study was to investigate how high temperatures affect the chemical composition of pollen grain surface in field pea using MIR spectroscopy with the goal of identifying traits conferring high temperature tolerance. Fresh, mature pollen grains from four replications of two commercially grown field pea cultivars, 'CDC Golden' (Warkentin et al. 2004) and 'CDC Sage' (Warkentin et al. 2006), were collected from buds on the fourth day of flower opening when exposed to two temperature regimes (24/18 °C vs. 35/18 °C day/night, 16 h photoperiod). Pollen grains were dusted on CaF_2 windows and the surface composition was analyzed using ATR-FTIR with the globar light as the infrared source, as described previously (Lahlali et al. 2014; Jiang et al. 2015).

The chemical composition (lipid, proteins, and carbohydrates) of pollen coat and exine of 'CDC Golden' (heat stress sensitive) and 'CDC Sage' (heat stress resistant) responded differently to elevated temperatures. In the protein region (1800–1500 cm^{-1}), the amount of α-helical structures (43.6%–48.6%) in pea pollen coat and exine was greater than β-sheets (41.3%–46.0%) in 'CDC Sage' (Lahlali et al. 2014). In contrast, 'CDC Golden' had a greater proportion of β-sheets (46.3%–51.7%) compared with α-helical structures (35.3%–36.2%) (Lahlali et al. 2014). Therefore, 'CDC Sage' had a higher α to β ratio than 'CDC Golden' (Lahlali et al. 2014).

In the lipid region, two strong negative peaks were observed near 2921 cm^{-1} (asymmetrical CH_2) and 2852 cm^{-1} (symmetrical CH_2) in the secondary derivative of absorption spectra. Both cultivars contained different amounts of two types of lipids on the pollen grain surface. The principal component primary axis analyses distinguished 'CDC Golden' and 'CDC Sage' as two separate clusters on the positive and negative sides via principal component analysis. The lipid region of the pollen grain surface of 'CDC Sage' was more stable than 'CDC Golden' under heat stress (Jiang et al. 2015).

In vitro pollen germination percentage of 'CDC Sage' was significantly greater than 'CDC Golden' after 10 h incubation at 36 °C (Jiang et al. 2016). Similarly, pollen viability of 'CDC Sage' at the anthesis stage was significantly higher than that of 'CDC Golden' when exposed to high temperature (35/18 °C) for 4 d (Y. Jiang et al., unpublished data). A greater in vitro pollen germination percentage and pollen viability in 'CDC Sage' may be associated with more stable lipid composition in pollen coat and exine compared with 'CDC Golden'. Lipids on pollen coats allow pollen tubes to penetrate the stigmatic papillae (Wolters-Arts et al. 1998). Additionally, because α-helical structures prevent bulk protein in pollen grains from the destructive effects of dehydration (Wolkers and Hoekstra 1995), the higher ratio of α-helical secondary protein structures to β-sheets in 'CDC Sage' compared with 'CDC Golden' may be another mechanism of high temperature tolerance.

Lipid composition in the pollen coat and exine layers was more stable in 'CDC Sage' than 'CDC Golden' when exposed to elevated temperatures. 'CDC Sage' also had a higher ratio of α-helical structures to β-sheets compared with 'CDC Golden'. More stable pollen surface lipids and the protein richness with α-helical structures seen in 'CDC Sage' may explain the unexpected finding that 'CDC Sage' had more heat-tolerant pollen grains compared with 'CDC Golden' (Lahlali et al. 2014; Jiang et al. 2015). FTIR spectroscopy, which does not necessarily need a synchrotron, can also be used to screen a large range of pea germplasm samples to improve pollen resistance to heat. This technique has proven to be a powerful nondestructive analytical tool to detect compositional changes on the pollen grain surface in response to environmental stress that can be applied to other biological samples.

Analysis of cellular chemophenotypes using an FPA

Mid-infrared analyses have two end stations, ATR and FPA mapping, both of which can be used to develop nondestructive methods to investigate tissue-specific phenotypes. Unlike conventional infrared sources that assess single point measurements, FPA enables spectral mapping and spatial localization studies of biological molecules across samples (Heraud et al. 2007). Yu (2004) was one of the first to illustrate the advantages of synchrotron FTIR microspectroscopy in revealing the microstructural matrix of feed that may link to nutrient utilization and structure–chemical information studies. Tanino et al. (2013) provided one of the first examples of synchrotron FPA mapping in plant abiotic stress using intact onion (*Allium fistulosum* L.) tissues. The FPA-FTIR maps in the intact single cell onion (*A. fistulosum*) epidermal peel illustrated here were created in 1 × 2 (64 pixel × 64 pixel) tiles with the detector connected to the Hyperion 3000 microscope using a 36× objective and assessed on samples of increasing freezing resistance from plants grown at 20 °C and those cold-acclimated for up to 2 wk at 4 °C (Tanino et al. 2013).

In the Tanino et al. (2013) study, after 2 wk of cold acclimation, the LT_{50} (the temperature at which 50% of the cells survived) decreased from −10 °C to −30 °C. This decrease in LT_{50} corresponded with an increase in the ratio of α-helix to β-sheet secondary structures (Fig. 3). An increase in the α to β ratio has been linked to an increase in dehydrins (Graether et al. 2001). Representative three-dimensional FTIR spectral plots integrated over 963–1745 cm^{-1} corresponded to spectra that include pectin and cellulose vibrational modes in common onion (*Allium cepa* L.) epidermal peels (Wilson et al. 2000). Principle component analysis in combination with the FPA-FTIR mapping enabled the detection of the separation between the intracellular and

Fig. 3. FTIR-FPA mapping and analysis of non- and cold-acclimated onion epidermal cells. (A) Functional group mapping over 0, 1, and 2 wk of cold acclimation [in which the freezing resistance increased from an LT_{50} of −10 °C (0 wk) to −30 °C (2 wk acclimation)] of the ratio of the α-helix secondary structures to β-sheet secondary structures. The false colour ranges from low (green) to high ratios (red) and shows the relative concentrations of the two types of secondary structures. The cell outlines from the light micrographs highlight the position of at least one of the cells from the tissue for reference. (B) Functional group map of the ratio of the total carbohydrate band to the total ester band. The false colour ranges from low (dark blue) to high (red) ratios over 0, 1, and 2 wk of cold acclimation. Three-dimensional FTIR spectral plots integrated over 963–1745 cm^{-1} corresponding to spectra including pectin and cellulose vibrational modes in *Allium cepa* L. (Wilson et al. 2000) with (C) non-acclimated cells and (D) 2-wk-acclimated cells. Corresponding cells displayed under visible light are shown below. (E) Principle component analysis of acclimated apoplast (black), acclimated symplast (blue), non-acclimated apoplast (red), and non-acclimated symplast (green). Adapted from Tanino et al. 2013. [Colour online.]

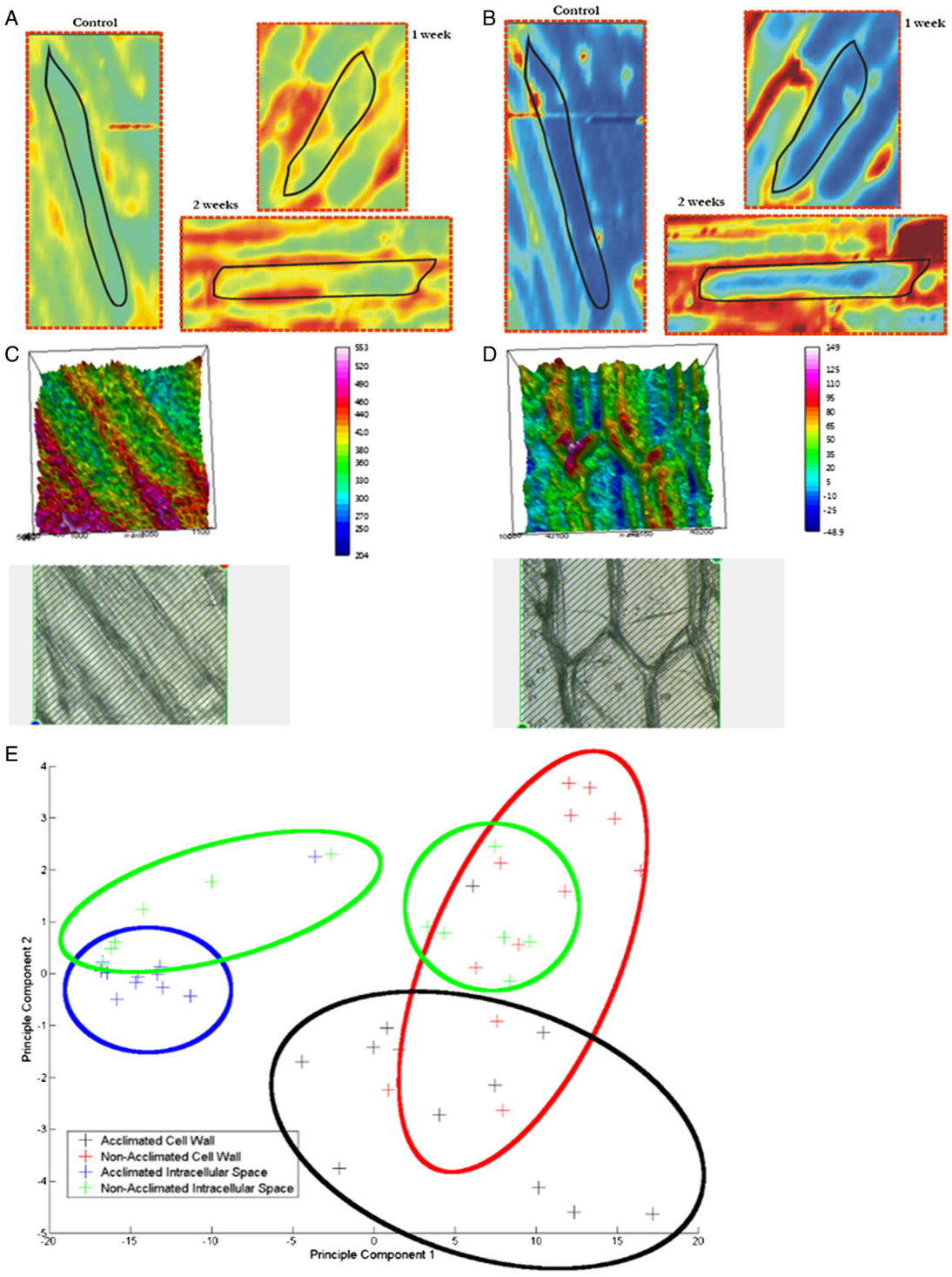

apoplastic spaces induced by acclimation (no overlap of blue and black circles) (Fig. 3).

The use of FTIR-FPA has also been applied to identify FHB biochemical traits in spring wheat by Lahlali et al. (2015, 2016*a*). Focal plane array mapping of rachis cross sections revealed a band (1710 cm^{-1}) associated with oxidative stress in the cell walls of epidermal and vascular bundle tissues in FHB-susceptible 'Muchmore' (DePauw et al. 2011) but not the resistant cultivar 'Sumai3' (Bai and Shaner 1994) after FHB infection (Lahlali et al. 2016*a*). 'Sumai3' was also identified to have higher peaks associated with lignin, hemicellulose and cellulose than in 'Muchmore'. This corresponds to visibly thicker rachis nodes in the 'Sumai3' spikelet in comparison to 'Muchmore', as visualized by synchrotron radiation two-dimensional phase contrast imaging (Lahlali et al. 2015). Similar research identifying peaks associated with environmental stress identified by synchrotron FTIR mapping has also been used to identify bands associated with protein degradation in wheat kernels as a result of frost (Xin et al. 2013) and fungal infection (Singh et al. 2011).

The intact onion epidermal peel and wheat spikelet rachis node examples illustrate the value of combining FPA with MIR to provide qualitative and quantitative spatial localization mapping of biological functional groups. The methods of sample preparation mentioned here are simple, cost effective, and noninvasive. Mid-infrared spectroscopy techniques also provide an opportunity to identify tissue-specific phenotypic markers associated with environmental stress.

Plant tissue barriers against pathogenic stress

Stripe rust of wheat caused by *Puccinia striiformis* f. sp. *tritici* Erikss. has been an issue in irrigated soft white spring wheat in southern Alberta (Su et al. 2003), and more recently in Canada Western Red Winter, Canada Western Red Spring, and Canada Prairie Spring Red wheat classes in western Canada (Puchalski and Gaudet 2011). Stripe rust in Saskatchewan is managed through the application of fungicides and selection of resistant wheat cultivars (Brar and Kutcher 2016). Although the adult plant resistance gene *Yr18*/*Lr34* is present in most modern varieties, only a few seedling resistance genes, including *Yr17*, *Yr10*, and *Yr27*, have been deployed in Canadian wheat cultivars (Puchalski and Gaudet 2011; Randhawa et al. 2012).

Studies on modifications to cell wall biopolymers of infected plants due to stripe and leaf rust are scarce. The cell wall forms a passive barrier in that extensive wall degradation is required by invading pathogens for infection to spread and can serve as a reservoir of antimicrobial compounds (reviewed by Zhao and Dixon 2014). In the past, similar biopolymeric modifications have been noted using FTIR spectroscopy in the rachis of resistant and susceptible spring wheat following exposure to FHB, caused by *F. graminearum* (Teleomorph: *Gibberella zeae* (Schwein.) Petch; Lahlali et al. 2015, 2016*a*, 2016*b*). The objectives of this study were to understand changes in cell wall biopolymers following infection in resistant and susceptible wheat cultivars and to determine whether these modifications can act as biochemical markers for stripe rust damage. Specifically, the effect of *P. striiformis* inoculation on the degree of pathogenic resistance in relationship to alterations in cell wall biopolymers was investigated using near-isogenic lines in 'Avocet', background differentiating for gene *Yr10* (Brar and Kutcher 2016). The gene *Yr10* was chosen for study as this seedling resistance gene is still effective to the majority of *P. striiformis* races existing in Saskatchewan (Brar et al. 2017). Two *P. striiformis* isolates, W047 (avirulent) and W053 (virulent), were inoculated onto the leaves of 10-d-old seedlings of 'Avocet' wheat isogenic lines with and without *Yr10* (Brar and Kutcher 2016). Leaves collected at 15 d after inoculation were freeze dried, ground into a powder, and then analyzed using the KBr pellet method.

Increases in cell wall lignin abundance have been correlated with reduced spread of *P. striiformis* in resistant wheat cultivars (Moldenhauer et al. 2006). Preliminary research shows that increases in cellulose, xylan, phenolic, and aromatic compounds were equally important in the *Yr10* near-isogenic line (Lahlali et al. 2016*b*). Although gene *Yr10* has been cloned (Liu et al. 2014), the complete mechanism of resistance is still unclear and the results from the present study may not necessarily be related to *Yr10* functioning, but to basal resistance in wheat against *P. striiformis*. Preliminary results from the study distinguished biopolymeric changes between compatible and incompatible interactions using FTIR. Thus, FTIR can potentially be used to study major biopolymers such as lignin, pectin, xylans, and lipids that are involved in biotic stress.

Protein secondary structures as markers for freezing tolerance in winter wheat

The critical region for the winter survival of winter wheat (*T. aestivum*) is the crown (Chen et al. 1983; Tanino and McKersie 1985). One of the mechanisms of crown freezing tolerance that cold-acclimated winter cereals employ is the secretion of antifreeze proteins to inhibit damage caused by ice propagation within the extracellular space (Griffith et al. 2005). Plant antifreeze proteins can be identified by their secondary structures. The ratio of α-helices to β-sheets has been used as a biochemical marker for Type I antifreeze proteins in animals (Graether et al. 2001); feeds (Yu 2004), and in plants such as the Japanese bunching onion (Tanino et al. 2013). Quantifying specific antifreeze proteins through conventional immunoblotting or proteomic analysis is both time consuming and expensive. For preliminary identification, FTIR spectroscopy analysis requires only minimal sample preparation, is rapid, and, with curve fitting models, can provide information on protein secondary structures (Goormaghtigh et al. 1990).

Table 1. Secondary structure characteristics of protein from non- and cold-acclimated 'Norstar' winter wheat crowns (n = 10) identified by FTIR spectroscopy.

Secondary structure (peak intensity a.u.)	Non-acclimated	Cold-acclimated	SEM	P value
α-helix	0.125b	0.237a	0.011	<0.0001
β-sheet	0.256a	0.141b	0.011	<0.0001
β-turn	0.139a	0.065b	0.009	<0.0001
Random coil	0.123a	0.014b	0.015	<0.0001
α-helix: β-sheet	0.501b	1.757a	0.081	<0.0001

Note: Means were separated according to the Tukey's honest significant difference (HSD) test (I.R. Willick, unpublished data). Means not sharing a lowercase letters differ significantly at the $P < 0.05$ level. SEM, standard error of the mean.

The objective of this study (I.R. Willick et al., unpublished data) was to investigate the effects of cold acclimation on the induction of antifreeze proteins in 'Norstar' winter wheat using MIR spectroscopy. This application highlights synchrotron tools that can analyze not only composition but secondary protein structure in the same biological tissue sample, particularly where small amounts of tissue are available in a short time period. 'Norstar' winter wheat (Grant 1980) was grown hydroponically as previously described (Limin and Fowler 2002). Seedlings were established for 14 d in hydroponic tanks containing half-strength Hoagland's solution at 20 °C with a 16 h photoperiod and a photosynthetic photon flux density (PPFD) of 300 μmol m^{-2} s^{-1} (non-acclimated). Half of the plants were transferred to a 4 °C chamber with a 16 h photoperiod and a PPFD of 250 μmol m^{-2} s^{-1} (cold-acclimation). Ten non-acclimated and 10 cold-acclimated plants were selected. Crowns were excised, frozen in liquid nitrogen, and ground into a fine powder in a chilled mortar. Samples were freeze dried for 72 h and then stored at −80 °C until analyzed. Samples were prepared and analyzed using the KBr method as described previously (Lahlali et al. 2015). Each infrared spectrum (an average of 256 scans) was recorded in the MIR range (4000–800 cm^{-1}) with a spectral resolution of 4 cm^{-1}. Curve fitting for each protein secondary structure was conducted as per Goormaghtigh et al. (1990). Statistical analysis was performed using the PROC GLM statistical package of SAS 9.3 (SAS Institute Inc., Cary, NC). Analysis of variance with the Tukey's test ($P < 0.05$) was used for mean comparisons (Table 1).

The chemical composition of the amide I protein region (1800–1700 cm^{-1}) in 'Norstar' crowns responded differently in non- and cold-acclimated treatments. The α-helical peak height was significantly higher in cold as opposed to non-acclimated crowns ($P < 0.05$; Table 1). In contrast, the β-sheet peak height significantly decreased due to the cold-acclimation treatment ($P < 0.05$; Table 1). The α-helical to β-sheet ratio was significantly greater in 'Norstar' crowns after 42 d of cold acclimation. This increase in the α to β ratio during cold acclimation corresponds with increases in antifreeze protein abundance (glucanases, thaumatin-like proteins, and defensins) within extracellular protein fraction extracts (I.R. Willick, unpublished data). Similar increases in proteins with antifreeze properties have been observed in the extracellular fluids collected from cold-acclimated 'Puma' rye (*Secale cereale* L.) leaves (Griffith et al. 2005) and cold-acclimated 'Jackson' winter wheat crowns (Herman et al. 2006). An increase in antifreeze proteins has been associated with the modification of ice within the vascular tissue at the base of the crown (Olien 1964). By binding to one or more growing planes of the ice crystal, the antifreeze proteins change the crystal shape and reduce the degree of damage (Jia and Davies 2002). The results of this study indicate that FTIR spectroscopy can be used to characterize the α to β ratio in 'Norstar' winter wheat. A large-scale field study amongst multiple winter wheat genotypes with contrasting freezing resistance is required to determine the applicability of the protein molecular structures studied as a biochemical marker for freezing resistance.

Animal feed quality

Novel research ideas and tools have played a significant role in advances in feed science and animal nutrition research (Yu 2004). Advanced synchrotron-based analytical technology was used to study feed molecular structure and structure changes induced by various processing and treatments (such as gene-transformation, bioethanol processing, and heat processing) in relation to nutrient utilization and availability in the animal. Unlike conventional wet analytical methods, these synchrotron-based techniques have been developed as rapid, nondestructive, and bioanalytical techniques that do not alter intrinsic feed structures. There has been little application of synchrotron radiation-based infrared microspectroscopy to the understanding of the inherent structures and nutrient availability of animal feed by the animal science community. This bioanalytical technique takes advantage of synchrotron light brightness and can explore molecular chemistry as well as the structure of biological tissues at ultra-high spatial resolutions without destroying inherent structures (Yu 2004; Marinkovic and Chance 2006; Miller and Dumas 2006).

The applications of synchrotron technology in feed and animal nutrition research have included (*i*) feed molecular structure in relation to nutrient availability; (*ii*) feed molecular-chemical makeup and micronutrient localization; (*iii*) feed molecular chemistry imaging; (*iv*) effect of gene transformation on feed structure; (*v*) heat-induced changes in structure and relation to nutrient availability; and (*vi*) the effect of bioethanol processing on feed structure and quality (Yu 2005*a*, 2005*b*, 2005*c*; Becker and Yu 2013; Yang et al. 2013; Yu et al. 2013).

Nutritional profiling of pea seeds

Wet bench biochemical analysis and atomic absorption spectroscopy are popular methods used to quantify organic and mineral composition of seeds. Both these methods involve homogenization and extraction, often followed by chemical modification of the extracts before the target compound or mineral can be quantified (Sharma et al. 2015), with cost often charged on a per element per sample basis. Because wet bench methods require multiple, time consuming, and expensive measurements, biochemical and nutritional traits of crops are neither routinely nor extensively used in current crop variety development.

A rapid and low cost nutritional profiling method to accurately measure a wide range of nutritional elements of the grain would set the stage for high-throughput evaluation of large breeding populations and germplasm collections. Such methods for biochemical and or nutritional profiling could be implemented in the month after harvest each year, providing timely data for selection of desirable breeding lines. Although near-infrared (NIR) spectroscopy is often used to predict protein and starch concentrations in seed powders (Esteve-Agelet et al. 2012), it has the disadvantage that it relies on absorption bands that are weak and diffuse with overlapping overtones of the sharper and relatively stronger primary absorbance bands of compounds in the MIR spectral region. As a consequence, NIR absorbance bands of multiple compounds may overlap (Wilks 2006). Therefore, NIR-based quantification of biochemical components in complex systems like tissue samples depends on elaborate calibration procedures that are not easily transferable from instrument to instrument. In contrast, MIR spectroscopy can generate sharper and stronger absorbance peaks with a greater signal to noise ratio, representing specific biochemical compounds. Similarly, XRF spectra generated directly from seed powders can be analyzed to semi-quantitatively estimate mineral composition of seeds (Miller and Dumas 2006; Iwai et al. 2012). The objective of this study was to elucidate the chemical composition of field pea seeds using XRF and MIR spectroscopy.

Seeds from 'CDC Bronco' field pea (Warkentin et al. 2005) were dried and ground into a fine powder with a quartz mortar and pestle to avoid metal contamination, and then stored in a desiccator. Approximately 10 mg

Fig. 4. Average FTIR (2800–900 cm^{-1}) (A) spectra and (B) XRF profiles collected from whole 'CDC Bronco' mature seeds. The FTIR spectra were an average of nine spectra from three biological samples collected from KBr pellets. The XRF profile was an average of six spectra from three biological samples.

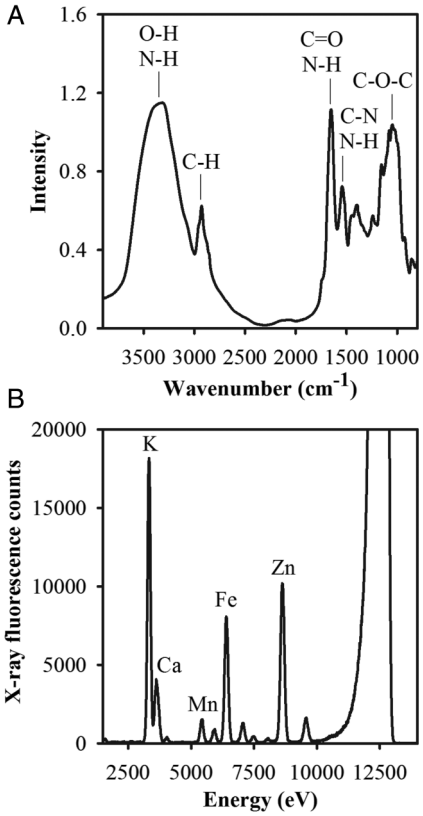

powdered samples of XRF were packed in an X-ray transparent slit of 0.5 cm × 3.0 cm made using a Teflon plate. Data collection was accomplished using Acquaman control software with a dwell time of 180 s. Incident and transmitted X-ray fluxes were measured using the upstream and downstream ionization chamber currents. The XRF data was normalized to the standard ring current of 250 mA and then plotted using Origin software (version 9.1, OriginLab Corporation, Northampton, MA).

The MIR absorption spectra collected from 'CDC Bronco' seeds represent the relative absorption of infrared radiation by the samples between 4000 and 600 cm^{-1} and contain all of the major spectral features found in biological samples (Fig. 4). A broad peak between 3500 and 3300 cm^{-1} represents –OH stretching vibration and water content. In plant tissues, some of this spectral signal also represents the –OH groups of carbohydrates. The region between 3000 and 2800 cm^{-1} represent lipids ($-CH_3$, $-CH_2$ stretching vibrations). The two prominent sharp peaks in the 1700–1600 and 1600–1500 cm^{-1} regions of the MIR absorbance spectrum represent amide I and amide II vibrations of proteins and have been used to precisely quantify proteins.

A 1510 cm^{-1} shoulder on the amide II peak corresponds to the lignin aromatic ring vibration.

The spectral features in the region 900–1250 cm^{-1} broadly represent the C–O–C, C–C, and P–O vibrations found in polysaccharides and phosphates of plant samples. As expected, all the pea seed powder samples exhibit peaks representing protein, lipid, carbohydrate and phosphate compounds. We have also identified four very strong peaks at 980, 966, 931, and 841 cm^{-1} in the MIR absorption spectra of pea seed powders that represent the P–O–C asymmetric stretch; a weak peak at 2927 cm^{-1} representative of the –OH stretch of phosphorus oxy acids; and a broad peak from 1158 to 1126 cm^{-1}. In addition, we identified two specific peaks at 1087 and 1071 cm^{-1} related to the P = O stretch vibrations.

Furthermore, the averaged XRF spectra (Fig. 4B) of pea seeds indicates that Zn, Ca, Fe, K, and Mn content can be measured in parallel from the same seed samples, without time consuming extraction steps. The results generated through this study give us confidence that reliable data on organic nutritional and anti-nutritional components of seeds such as proteins, starch, and phytic acid can be effectively combined with valuable complementary information on mineral composition of pea and other crop seeds using the resources available in a synchrotron facility such as CLS.

Similar phytic acid based studies using XRF and micro-XRF imaging have been conducted in rice (*Oryza sativa* L.). Over the course of seed development, phytic acid accumulated in the aleurone layer and the endosperm (Iwai et al. 2012). Using XRF imaging, Iwai and colleagues showed Ca, K, and Fe co-localized with phytic acid, Zn was loosely bound, and Cu accumulated in the endosperm but did not co-localize with phytate (Iwai et al. 2012). Transgenic rice lines with low phytic acid had reduced P and K in the aleurone layer and a greater localization of Zn and Cu to only the aleurone layer in comparison to the nontransgenic control (Sakai et al. 2015). Synchrotron XRF imaging has also been used as a proof of principle in seed transformation studies (Menguer et al. 2017). Menguer and colleagues transformed barley (*Hordeum vulgare* L.) to express a Zn transporter (HvMTP1) and used XRF imaging to confirm the redistribution of Zn from the aleurone to the endosperm.

These studies provide a gateway into the process of localizing mineral nutrients to specific tissue compartments and correlating the localization with their chemical status. This can provide valuable insight into the nutritional and processing aspects of crop utilization. Once validated, breeders, biotechnologists, and processors will be able to utilize this information to devise knowledge-based strategies to improve the nutritional composition of seeds and seed-based products. For example, the analysis of the phosphate-related peaks in the 1158–1126 cm^{-1} range have been used to distinguish between normal and low phytic acid mutants of pea (P. Vijayan and B. Smith, unpublished data) and can subsequently lead to the development of high-throughput methods for screening biochemical phenotypes of interest.

Table 2. Semi-quantitative rhodium-normalized calcium (Ca), potassium (K), phosophorus (P), and sulfur (S) contents measured using a portable X-ray fluorometer at proximal, central, and distal peel locations and the cortex of *Malus pumila* Mill. 'Honeycrisp' (n = 142).

Tissue	Ca	K	P	S
Proximal	0.289c	0.295d	0.0161c	0.0453b
Center	0.262b	0.273b	0.0152b	0.0451b
Distal	0.273bc	0.284c	0.0158c	0.0451b
Cortex	0.043a	0.133a	0.0102a	0.0255a

Note: Means were separated using Tukey's HSD test. Means not sharing a lowercase letter differ significantly at the $P < 0.05$ level.

Handheld technology and field applications

The transport of nutrients into developing fruit is dependent on transpirational water flow in addition to ion transport mechanisms. Upon transfer from the xylem to surrounding cells, the mobility of calcium is a function of the combined symplastic and apoplastic flow (Gilliham et al. 2011). Using ^{45}Ca radioisotope, Shear and Faust (1970) illustrated that calcium mobility is limited in plant tissue once it is unloaded from the xylem. Differences in the distribution of xylem vessels and functionality over time (Dražeta et al. 2004; Miqueloto et al. 2014) can cause significant spatial variability in plant tissue elemental concentrations. This has been shown using traditional elemental analysis (Ferguson and Watkins 1983) as well as nondestructive analysis (Kalcsits 2016). Recent advancements in photometry have increased the resolution at which spatial differences in microstructure affecting calcium mobility can be measured. Synchrotron or conventional XRF can be used for tissue level analysis (McLaren et al. 2012; Kalcsits 2016) or to localize elemental concentrations at a cellular level (Zhao et al. 2014). Synchrotron XRF provides micron-scale resolution for mapping elemental distribution in plant samples. However, handheld XRF provides opportunities for in situ analysis that, in combination with synchrotron XRF, can provide important information on how elemental distribution affects the development of Ca-related disorders. The objective of this work was to nondestructively identify variation in Ca, K, S, and P concentration in the proximal, middle, and distal regions of apple and pear using handheld XRF.

'Honeycrisp' apples with a range in sizes from a commercial packing facility were analyzed using a Bruker AXS Tracer 3-V portable handheld x-ray fluorometer (PXRF) analyzer (Bruker Elemental, Kennewick, WA). The PXRF was equipped with a rhodium tube from which X-rays are emitted and a Peltier-cooled silicon

Fig. 5. Smoothed semi-quantitative potassium to calcium ratio on the surface of an apple affected by bitter pit (left) and a healthy apple (right) calculated as the rhodium-normalized PXRF counts for potassium divided by the rhodium-normalized PXRF counts for calcium. The potassium to calcium ratio was twice as high in the apple affected by bitter pit than in the healthy apple, with differences in spatial distribution. Adapted from Kalcsits (2016). [Colour online.]

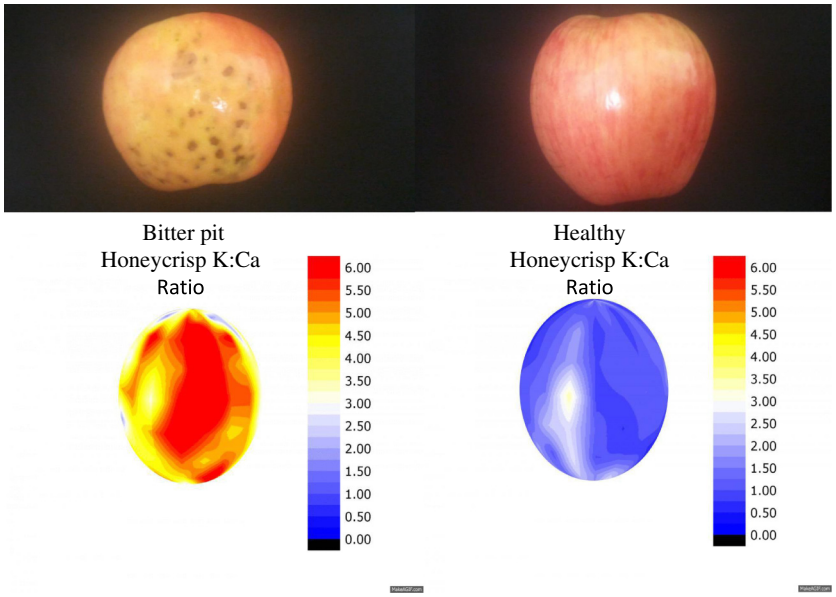

PIN diode detector operating at 15 kV and 25 μA from an external power source for 15 s using no filter under a vacuum at <10 torr. X-ray counts were processed using the S1PXRF spectra program developed by Bruker in a semi-quantitative approach for measuring Ca, K, S, and P. Each fruit was measured at 12 spots; 4 from each of the calyx, equator, and stem end. More detail on this method can be found in Kalcsits (2016).

With the handheld device, Ca, K, and P were found to be significantly different among regions of the apple (Table 2). Both Ca and K were greatest at the proximal and distal regions of the fruit. Sulfur was not significantly different along the fruit surface. The cortex had significantly lower elemental content than the peel; however, the greatest difference between the peel and the cortex was for Ca, where the rhodium-normalized, semi-quantitative Ca content was between 0.262 and 0.289 in the peel and 0.043 in the cortex. This difference is perhaps best exemplified in bitter pit affected fruit compared with healthy fruit, as shown when K to Ca ratios are mapped (Fig. 5, from Kalcsits 2016). Detecting the variation in elements at the whole plant, tissue, and cellular levels is critical to understanding the factors that affect these distribution patterns. Using XRF, significant variation in Ca, K, P, and S concentrations in both apple and pear were identified at the tissue level. While differences in these concentrations were significant, calibrations are not available for quantitative analysis of plant tissue, limiting measurements to relative comparisons among treatments. Depending on the type of XRF, the measurement resolution can be >1 cm for tissue-level analyses or as small as 50 nm for subcellular analyses. For many horticultural crops, the overall Ca concentration in plant tissue and its ratio to other elements such as K, Mg, and N have been implicated as a predictor of Ca deficiency-related physiological disorders (White and Broadley 2003). However, Kalcsits (2016) reported the K to Ca ratios vary significantly along the fruit surface (Tables 2 and 3; Fig. 5). Current analytical practices suggest pooling of fruit within an orchard masks the variation in elemental distribution between and within fruit that may contribute to Ca-related disorders. De Freitas et al. (2012) suggested the amount of free apoplastic Ca may affect the development of bitter pit symptoms. Calcium is primarily distributed throughout the cell wall, cytoplasm, and vacuole, with much of the Ca present in the cell wall and vacuole and cytoplasmic Ca concentrations tightly regulated (Hocking et al. 2016). The amount of variation that exists within a fruit at the cellular level and the factors that contribute to this variation are less understood. Using micro-XRF to determine the in situ cellular distribution and speciation of Ca in apples (and other fruit suffering from Ca-related disorders) would significantly advance research in this area and lead to viable and cost-efficient solutions.

Use of XRF has the potential to provide insight into factors that affect overall distribution of elements at the whole plant and cellular levels. The ability to measure this variation may provide answers to some of the underlying causes of Ca-related problems in horticultural crops. The trends in elemental concentrations

Table 3. Semi-quantitative rhodium-normalized calcium (Ca), potassium (K), phosphorus (P), and sulfur (S) content measured using a portable X-ray fluorometer of peel and cortex tissue at stem and bottom locations of *Pyrus communis* 'Bartlett' and 'Starkrimson' ($n = 160$).

	Tissue	Ca	K	P	S
Bartlet					
Stem	Peel	0.203d	0.583c	0.020b	0.039b
	Cortex	0.113b	0.230a	0.009a	0.020a
Bottom	Peel	0.168c	0.428b	0.019b	0.043c
	Cortex	0.051a	0.224a	0.010a	0.022a
Starkrimson					
Stem	Peel	0.138d	0.640b	0.022b	0.037b
	Cortex	0.085b	0.217a	0.008a	0.016a
Bottom	Peel	0.106c	0.617b	0.029c	0.044c
	Cortex	0.044a	0.138a	0.008a	0.018a

Note: Means were separated using Tukey's HSD test. Means not sharing a lowercase letter differ significantly at the $P < 0.05$ level.

among different regions of the fruit were similar for both 'Bartlett' and 'Starkrimson' pears. Similar to apple, concentrations of Ca, K, P, and S (Table 3) were greater in the peel than the cortex. The differences between the stem end and bottom (distal, calyx end) of the pear were greater than they were for apple. Calcium concentrations were lower and K concentrations higher in 'Starkrimson' than 'Bartlett' pears in all regions except the cortex in the bottom of the fruit ($P < 0.05$).

Reports in the literature indicate that use of handheld FTIR devices have been applied sparingly in soil (Forrester et al. 2015) and plant sciences (Wilkerson et al. 2013). For example, in Australia, the P buffer index is an important measurement used in determining rates of P application for optimum crop yield while preventing environmental pollution due to excessive use of fertilizers. Samples can be analyzed using FTIR to quantify the P buffer index; however, this requires samples to be shipped to the lab for analysis (Forrester et al. 2015). The possibility of on-site testing would improve efficiency. Using partial least squares regression of spectra obtained from Australian soils showed that accuracy and high signal to noise ratio (Forrester et al. 2015) of handheld MIR device spectra were comparable to results from benchtop analyses.

Portable infrared units would provide plant breeders with a powerful tool for rapid assessment of quality attributes, such as sugar content in tomatoes or the identification of injury in harvested material or field plants that are unidentifiable upon visual inspection. From an industry perspective, rapid analysis of plant byproducts would allow for timely corrective measures during manufacturing and processing. With the use of partial least square regression calibration models, handheld models accurately estimated sugar, acidity, and soluble solid quality parameters in tomato juice processed from plant breeding lines to the same degree as conventional measurements (gas chromatography, titration, Brix meters) and benchtop FTIR machines (Wilkerson et al. 2013). Similar partial least square regression models can be applied to specific biochemical markers such as protein peaks to assess for kernel quality (Singh et al. 2011; Xin et al. 2013) or absorbance peaks associated with oxidative stress (Lahlali et al. 2016*a*, 2016*b*). In the future, programs accompanying these handheld devices could be used to detect early injury or infection in field plants that is not visible to the naked eye and ultimately be used to differentiate susceptible and resistant breeding material.

Conclusions

Synchrotron technology is a promising powerful tool in plant sciences with distinct advantages over other technologies, particularly in areas such as ease of sample preparation, nutrient profiling, compositional analysis, and nondestructive mapping, enabling spatial localization of biological molecules and evaluation of protein secondary structures. Synchrotron technology is both a useful first approach to determine broad differences for further detailed investigation through complementary technology and in providing detailed analytical compositional information. Existing tools such as handheld XRF units illustrate the value of nondestructive, high-throughput approaches. Increasingly, synchrotron technology is also incorporating techniques to better address the high-throughput needs of plant breeding programs.

Acknowledgements

We thank the Canadian Society of Horticultural Sciences for their invitation to present and publish this paper. Research presented in this paper was conducted at the CLS, which is funded by the Canada Foundation for Innovation, the Natural Sciences and Engineering Research Council of Canada, the National Research Council Canada, the Canadian Institutes of Health Research, the Government of Saskatchewan, Western Economic Diversification Canada, and the University of Saskatchewan. We acknowledge the Saskatchewan Agriculture Development Fund, the Saskatchewan Pulse Growers Association Fund, and the Western Grains Research Fund. Funding for the X-ray fluorometer experiments by L. Kalcsits was partially supported by the Washington Tree Fruit Research Commission. We would also like to acknowledge the assistance of the CLS beamline scientists, both past and present, for their assistance.

References

Bai, G., and Shaner, G. 1994. Scab of wheat: prospects for control. Plant Dis. **78**: 760–766. doi:10.1094/PD-78-0760.

Becker, P.M., and Yu, P. 2013. What makes protein indigestible from tissue-related, cellular, and molecular aspects? Mol. Nutr. Food Res. **57**: 1695–1707. doi:10.1002/mnfr.201200592. PMID:23765989.

Bird, S.M., and Gray, J.E. 2003. Signals from the cuticle affect epidermal cell differentiation. New Phytol. **157**: 9–23. doi:10.1046/j.1469-8137.2003.00543.x.

Brar, G.S., and Kutcher, H.R. 2016. Race characterization of *Puccinia striiformis* f. sp. *tritici*, the cause of wheat stripe rust, in Saskatchewan and Southern Alberta, Canada and virulence comparison with races from the United States. Plant Dis. **100**: 1744–1753. doi:10.1094/PDIS-12-15-1410-RE.

Brar, G.S., Graf, R., Knox, R., Campbell, H., and Kutcher, H.R. 2017. Reaction of differential wheat and triticale genotypes to natural stripe rust [*Puccinia striiformis* f. sp. *tritici*] infection in Saskatchewan, Canada. Can. J. Plant Pathol. **39**(2): 138–148. doi:10.1080/07060661.2017.1341433.

Buddenhagen, I.W. 1983. Breeding strategies for stress and disease resistance in developing countries. Annu. Rev. Phytopathol. **21**: 385–409. doi:10.1146/annurev.py.21.090183.002125.

Chen, T.H.-H., Gusta, L.V., and Fowler, D.B. 1983. Freezing injury and root development in winter cereals. Plant Physiol. **73**: 773–777. doi:10.1104/pp.73.3.773. PMID:16663299.

de Freitas, S.T., Handa, A.K., Wu, Q., Park, S., and Mitcham, E.J. 2012. Role of pectin methylesterases in cellular calcium distribution and blossom-end rot development in tomato fruit. Plant J. **71**: 824–835. doi:10.1111/j.1365-313X.2012.05034.x. PMID:22563738.

DePauw, R.M., Knox, R.E., McCaig, T.N., Clarke, F.R., and Clarke, J.M. 2011. Muchmore hard red spring wheat. Can. J. Plant Sci. **91**(4): 797–803. doi:10.4141/cjps10188.

Dickinson, H. 1993. Pollen dressed for success. Nature, **364**: 573–574. doi:10.1038/364573a0.

Dražeta, L., Lang, A., Hall, A.J., Volz, R.K., and Jameson, P.E. 2004. Causes and effects of changes in xylem functionality in apple fruit. Ann. Bot. **93**: 275–282. doi:10.1093/aob/mch040. PMID:14988096.

DuPont Pioneer. 2017. Corn in Western Canada. [Online]. DuPont Pioneer, Johnston, IA. Available from https://www.pioneer.com/home/site/ca/products/corn/western_canada_corn/?site=saskatoon.

Esteve-Agelet, L., Armstrong, P.R., Clariana, I.R., and Hurburgh, C.R. 2012. Measurement of single soybean seed attributes by near-infrared technologies. A comparative study. J. Agric. Food. Chem. **60**: 8314–8322. doi:10.1021/jf3012807. PMID:22831652.

Ferguson, I.B., and Watkins, C.B. 1983. Cation distribution and balance in apple fruit in relation to calcium treatments for bitter pit. Sci. Hort. **19**: 301–310. doi:10.1016/0304-4238(83)90078-X.

Fiorani, F., and Schurr, U. 2013. Future scenarios for plant phenotyping. Annu. Rev. Plant Biol. **64**: 267–291. doi:10.1146/annurev-arplant-050312-120137. PMID:23451789.

Food and Agriculture Organization of the United Nations. 2013. Crop water information: maize. [Online]. FAO, Rome, Italy. Available from http://www.fao.org/nr/water/cropinfo_maize.html.

Forrester, S.T., Janik, L.J., Soriano-Disla, J.M., Mason, S., Burkitt, L., Moody, P., Gourley, C.J., and McLaughlin, M.J. 2015. Use of handheld mid-infrared spectroscopy and partial least-squares regression for the prediction of the phosphorus buffering index in Australian soils. Soil Res. **53**: 67–80. doi:10.1071/SR14126.

Gilliham, M., Dayod, M., Hocking, B.J., Xu, B., Conn, S.J., Kaiser, B.N., Leigh, R.A., and Tyerman, S.D. 2011. Calcium delivery and storage in plant leaves: exploring the link with water flow. J. Exp. Bot. **62**: 2233–2250. doi:10.1093/jxb/err111. PMID:21511913.

Goormaghtigh, E., Cabiaux, V., and Ruysschaert, J.-M. 1990. Secondary structure and dosage of soluble and membrane proteins by attenuated total reflection Fourier-transform infrared spectroscopy on hydrated films. Eur. J. Biochem. **193**: 409–420. doi:10.1111/j.1432-1033.1990.tb19354.x. PMID:2226461.

Graether, S.P., Slupsky, C.M., Davies, P.L., and Sykes, B.D. 2001. Structure of type I antifreeze protein and mutants in supercooled water. Biophys. J. **81**: 1677–1683. doi:10.1016/S0006-3495(01)75821-3. PMID:11509380.

Grant, M. 1980. Registration of Norstar wheat (Reg. No. 626). Crop Sci. **20**: 552. doi:10.2135/cropsci1980.0011183X0020000040042x.

Griffith, M., Lumb, C., Wiseman, S.B., Wisniewski, M., Johnson, R.W., and Marangoni, A.G. 2005. Antifreeze proteins modify the freezing process in planta. Plant Physiol. **138**: 330–340. doi:10.1104/pp.104.058628. PMID:15805474.

Gu, L., Hanson, P.J., Mac Post, W., Kaiser, D.P., Yang, B., Nemani, R., Pallardy, S.G., and Meyers, T. 2008. The 2007 Eastern US spring freeze: increased cold damage in a warming world? BioScience, **58**(3): 253–262. doi:10.1641/B580311.

Heraud, P., Caine, S., Sanson, G., Gleadow, R., Wood, B.R., and McNaughton, D. 2007. Focal plane array infrared imaging: a new way to analyse leaf tissue. New Phytol. **173**: 216–225. doi:10.1111/j.1469-8137.2006.01881.x. PMID:17176407.

Herman, E.M., Rotter, K., Premakumar, R., Elwinger, G., Bae, R., Ehler-King, L., Chen, S., and Livingston, D.P. 2006. Additional freeze hardiness in wheat acquired by exposure to −3 °C is associated with extensive physiological, morphological, and molecular changes. J. Exp. Bot. **57**: 3601–3618. doi:10.1093/jxb/erl111. PMID:16968883.

Hocking, B., Tyerman, S.D., Burton, R.A., and Gilliham, M. 2016. Fruit calcium: transport and physiology. Front. Plant Sci. **7**: 569. doi:10.3389/fpls.2016.00569. PMID:27200042.

Huth, F., Govyadinov, A., Amarie, S., Nuansing, W., Keilmann, F., and Hillenbrand, R. 2012. Nano-FTIR absorption spectroscopy of molecular fingerprints at 20 nm spatial resolution. Nano Lett. **12**: 3973–3978. doi:10.1021/nl301159v. PMID:22703339.

Iwai, T., Takahashi, M., Oda, K., Terada, Y., and Yoshida, K.T. 2012. Dynamic changes in the distribution of minerals in relation to phytic acid accumulation during rice seed development. Plant Physiol. **160**: 2007–2014. doi:10.1104/pp.112.206573. PMID:23090587.

Jia, Z., and Davies, P.L. 2002. Antifreeze proteins: an unusual receptor-ligand interaction. Trends Biochem. Sci. **27**: 101–106. doi:10.1016/S0968-0004(01)02028-X. PMID:11852248.

Jiang, Y. 2016. Effect of heat stress on pollen development and seed set in field pea. Ph.D thesis, University of Saskatchewan, Saskatoon, SK. 71 pp.

Jiang, Y., Lahlali, R., Karunakaran, C., Kumar, S., Davis, A.R., and Bueckert, R.A. 2015. Seed set, pollen morphology and pollen surface composition response to heat stress in field pea. Plant Cell Environ. **38**: 2387–2397. doi:10.1111/pce.12589. PMID:26081983.

Kalcsits, L.A. 2016. Non-destructive measurement of calcium and potassium in apple and pear using handheld X-ray fluorescence. Front. Plant Sci. **7**: 442. doi:10.3389/fpls.2016.00442. PMID:27092160.

Kazarian, S.G., and Chan, K.L.A. 2010. Micro- and macro-attenuated total reflection Fourier transform infrared spectroscopic imaging. Appl. Spectrosc. **64**: 135A–152A. doi:10.1366/000370210791211673.

Lahlali, R., Jiang, Y., Kumar, S., Karunakaran, C., Liu, X., Borondics, F., Hallin, E., and Bueckert, R. 2014. ATR–FTIR spectroscopy reveals involvement of lipids and proteins of intact pea pollen grains to heat stress tolerance. Front. Plant Sci. **5**: 747. doi:10.3389/fpls.2014.00747. PMID:25566312.

Lahlali, R., Karunakaran, C., Wang, L., Willick, I., Schmidt, M., Liu, X., Borondics, F., Forseille, L., Fobert, P.F., Tanino, K., Peng, G., and Hallin, E. 2015. Synchrotron based phase contrast X-ray imaging combined with FTIR spectroscopy

reveals structural and biomolecular differences in spikelets play a significant role in resistance to *Fusarium* in wheat. BMC Plant Biol. **15**: 24. doi:10.1186/s12870-014-0357-5. PMID:25628148.

Lahlali, R., Kumar, S., Wang, L., Forseille, L., Sylvain, N., Korbas, M., Muir, D., Swerhone, G., Lawrence, J.R., Fobert, P.R., Peng, G., and Karunakaran, C. 2016*a*. Cell wall biomolecular composition plays a potential role in the host type II resistance to Fusarium head blight in wheat. Front. Microbiol. **7**: 910. doi:10.3389/fmicb.2016.00910. PMID:27445995.

Lahlali, R., Brar, G.S., Qutob, D., Karunakaran, C., and Kutcher, H.R. 2016*b*. Spectral signatures of chemical changes in the wheat cell-wall resulting from stripe rust infection in compatible and incompatible near-isogenic lines. Phytopathol. **106**: 144 (Abstr.).

Leugers, A., Neithamer, D.R., Sun, L.S., Hetzner, J.E., Hilty, S., Hong, S., Krause, M., and Beyerlein, K. 2003. High-throughput analysis in catalysis research using novel approaches to transmission infrared spectroscopy. J. Comb. Chem. **5**(3):238–244. doi:10.1021/cc0200944. PMID:12739939.

Limin, A.E., and Fowler, D.B. 2002. Developmental traits affecting low-temperature tolerance response in near-isogenic lines for the vernalization locus *Vrn-A1* in wheat (*Triticum aestivum* L. em Thell). Ann. Bot. **89**: 579–585. doi:10.1093/aob/mcf102. PMID:12099532.

Liu, W., Frick, M., Huel, R., Nykiforuk, C.L., Wang, X., Gaudet, D.A., Eudes, F., Conner, R.L., Kuzyk, A., Chen, Q., Kang, Z., and Laroche, A. 2014. The stripe rust resistance gene *Yr10* encodes an evolutionary-conserved and unique CC-NBS-LRR sequence in wheat. Mol. Plant. **7**(12): 1740–1755. doi:10.1093/mp/ssu112. PMID:25336565.

Marinkovic, N.S., and Chance, M.R. 2006. Synchrotron infrared microspectroscopy. Pages 671–708 in R. Meyers, ed. Encyclopedia of molecular cell biology and molecular medicine. Vol. 13, 2nd ed. John Wiley and Sons Inc., Chichester, UK.

Martín, J., Solla, A., Woodward, S., and Gil, L. 2005. Fourier transform-infrared spectroscopy as a new method for evaluating host resistance in the Dutch elm disease complex. Tree Physiol. **25**: 1331–1338. doi:10.1093/treephys/25.10.1331. PMID:16076781d.

McCann, M., Chen, L., Roberts, K., Kemsley, E., Sene, C., Carpita, N., Stacey, N., and Wilson, R. 1997. Infrared microspectroscopy: sampling heterogeneity in plant cell wall composition and architecture. Physiol. Plant. **100**: 729–738. doi:10.1111/j.1399-3054.1997.tb03080.x.

McLaren, T.I., Guppy, C.N., and Tighe, M.K. 2012. A rapid and nondestructive plant nutrient analysis using portable x-ray fluorescence. Soil Sci. Soc. Am. J. **76**: 1446–1453. doi:10.2136/sssaj2011.0355.

Menguer, P., Vincent, T., Miller, A.J., Brown, J.K., Vincze, E., Borg, S., Holm, P.B., Sanders, D., and Podar, D. 2017. Improving zinc accumulation in barley endosperm using HvMTP1, a transition metal transporter. Plant Biotech. J. doi:10.1111/pbi.12749.

Miller, L.M., and Dumas, P. 2006. Chemical imaging of biological tissue with synchrotron infrared light. Biochim. Biophys. Acta. **1758**: 846–857. doi:10.1016/j.bbamem.2006.04.010. PMID:16781664.

Miqueloto, A., do Amarante, C.V.T., Steffens, C.A., dos Santos, A., and Mitcham, E. 2014. Relationship between xylem functionality, calcium content and the incidence of bitter pit in apple fruit. Sci. Hort. **165**: 319–323. doi:10.1016/j.scienta.2013.11.029.

Moldenhauer, J., Moerschbacher, B.M., and Van Der Westhuizen, A.J. 2006. Histological investigation of stripe rust (*Puccinia striiformis* f. sp. *tritici*) development in resistant and susceptible wheat cultivars. Plant Pathol. **55**: 469–474. doi:10.1111/j.1365-3059.2006.01385.x.

Monsanto Canada. 2013. Monsanto Canada embarks on bold plan to bring new crop options to western Canadian farmers. [Online]. Monsanto Canada Inc., Winnipeg, MB. Available from http://www.monsanto.ca/newsviews/Pages/NR-2013-06-24.aspx.

Olien, C.R. 1964. Freezing processes in the crown of 'Hudson' barley, *Hordeum vulgare* (L., emend. Lam.) Hudson. Crop Sci. **4**: 91–95. doi:10.2135/cropsci1964.0011183X000400010028x.

Puchalski, B., and Gaudet, D.A. 2011. 2010 Southern Alberta stripe rust survey. Can. Plant Dis. Surv. **91**: 69–70.

Randhawa, H., Puchalski, B.J., Frick, M., Goyal, A., Despins, T., Graf, R.J., Laroche, A., and Gaudet, D.A. 2012. Stripe rust resistance among western Canadian spring wheat and triticale varieties. Can. J. Plant Sci. **92**: 713–722. doi:10.4141/cjps2011-252.

Sakai, H., Iwai, T., Matsubara, C., Usui, Y., Okamura, M., Yatou, O., Terada, Y., Aoki, N., Nishida, S., and Yoshida, K.T. 2015. A decrease in phytic acid content substantially affects the distribution of mineral elements within rice seeds. Plant Sci. **238**: 170–177. doi:10.1016/j.plantsci.2015.06.006. PMID:26259185.

Sharma, S., Singh, N., Virdi, A.S., and Rana, J.C. 2015. Quality traits analysis and protein profiling of field pea (*Pisum sativum*) germplasm from Himalayan region. Food Chem. **172**: 528–536. doi:10.1016/j.foodchem.2014.09.108. PMID:25442588.

Shear, C.B., and Faust, M. 1970. Calcium transport in apple trees. Plant Physiol. **45**: 670–674. doi:10.1104/pp.45.6.670. PMID:16657371.

Singh, C.B., Jayas, D.S., Borondics, F., and White, N.D. 2011. Synchrotron based infrared imaging study of compositional changes in stored wheat due to infection with *Aspergillus glaucus*. J. Stored Prod. Res. **47**: 372–377. doi:10.1016/j.jspr.2011.07.001.

Su, H., Conner, R.L., Graf, R.J., and Kuzyk, A.D. 2003. Virulence of *Puccinia striiformis* f. sp. *tritici*, cause of stripe rust on wheat, in western Canada from 1984 to 2002. Can. J. Plant Pathol. **25**: 312–319. doi:10.1080/07060660309507084.

Tanino, K.K., and McKersie, B.D. 1985. Injury within the crown of winter wheat seedlings after freezing and icing stress. Can. J. Bot. **63**: 432–436. doi:10.1139/b85-053.

Tanino, K.K., Kobayashi, S., Hyett, C., Hamilton, K., Liu, J., Li, B., Borondics, F., Pedersen, T., Tse, H., Ellis, T., Kawamura, Y., and Uemura, M. 2013. *Allium fistulosum* as a novel system to investigate mechanisms of freezing resistance. Physiol. Plant, **147**: 101–111. doi:10.1111/j.1399-3054.2012.01716.x. PMID:23078395.

Vigh, L., Horváth, I., Farkas, T., Mustárdy, L.A., and Faludi-Dániel, Á. 1981. Stomatal behaviour and cuticular properties of maize leaves of different chilling-resistance during cold treatment. Physiol. Plant. **51**: 287–290. doi:10.1111/j.1399-3054.1981.tb04479.x.

Vijayan, P., Willick, I.R., Lahlali, R., Karunakaran, C., and Tanino, K.K. 2015. Synchrotron radiation sheds fresh light on plant research: the use of powerful techniques to probe structure and composition of plants. Plant Cell Physiol. **56**: 1252–1263. doi:10.1093/pcp/pcv080. PMID:26117844.

Walter, A., Liebisch, F., and Hund, A. 2015. Plant phenotyping: from bean weighing to image analysis. Plant Methods, **11**: 14. doi:10.1186/s13007-015-0056-8. PMID:25767559.

Warkentin, T.D., Vandenberg, A., Banniza, S., and Slinkard, A. 2004. CDC Golden field pea. Can. J. Plant Sci. **84**: 237–238. doi:10.4141/P03-116.

Warkentin, T.D., Vandenberg, A., Banniza, S., and Slinkard, A. 2005. CDC Bronco field pea. Can. J. Plant Sci. **85**: 649–650. doi:10.4141/P04-160.

Warkentin, T.D., Vandenberg, A., Banniza, S., Barlow, B., and Ife, S. 2006. CDC Sage field pea. Can. J. Plant Sci. **86**: 161–162. doi:10.4141/P05-110.

White, P.J., and Broadley, M.R. 2003. Calcium in plants. Ann. Bot. **92**: 487–511. doi:10.1093/aob/mcg164. PMID:12933363.

Willick, I.R., Lahlali, R., Vijayan, P., Muir, D., Karunakaran, C., and Tanino, K.K. 2017. Wheat flag leaf epicuticular wax morphology and composition in response to moderate drought stress are revealed by SEM, FTIR-ATR and synchrotron X-ray spectroscopy. Physiol. Plant. (in press). doi:10.1111/ppl.12637. PMID:28857201.

Wilkerson, E.D., Anthon, G.E., Barrett, D.M., Sayajon, G.F.G., Santos, A.M., and Rodriguez-Saona, L.E. 2013. Rapid assessment of quality parameters in processing tomatoes using hand-held and benchtop infrared spectrometers and multivariate analysis. J. Agric. Food Chem. **61**: 2088–2095. doi:10.1021/jf304968f. PMID:23373962.

Wilks, P. 2006. NIR versus mid-IR: how to choose. Spectroscopy, **21**(4).

Wilson, R.H., Smith, A.C., Kačuráková, M., Saunders, P.K., Wellner, N., and Waldron, K.W. 2000. The mechanical properties and molecular dynamics of plant cell wall polysaccharides studied by Fourier-transform infrared spectroscopy. Plant Physiol. **124**: 397–406. doi:10.1104/pp.124.1.397. PMID:10982452.

Wisniewski, M., and Fuller, M. 1999. Ice nucleation and deep supercooling in plants: new insights using infrared thermography. Pages 105–118 in R. Margesin and R. Schinner, eds. Cold-adapted organisms: ecology, physiology, enzymology and molecular biology. Springer, Berlin, Germany.

Wolkers, W.F., and Hoekstra, F.A. 1995. Aging of dry desiccation-tolerant pollen does not affect protein secondary structure. Plant Physiol. **109**: 907–915. doi:10.1104/pp.109.3.907. PMID:12228641.

Wolters-Arts, M., Lush, W.M., and Mariani, C. 1998. Lipids are required for directional pollen-tube growth. Nature, **392**: 818–821. doi:10.1038/33929. PMID:9572141.

Xin, H., Zhang, X., and Yu, P. 2013. Using synchrotron radiation-based infrared microspectroscopy to reveal microchemical structure characterization: frost damaged wheat vs. normal wheat. Int. J. Mol. Sci. **14**: 16706–16718. doi:10.3390/ijms140816706. PMID:23949633.

Yang, L., Christensen, D.A., McKinnon, J.J., Beattie, A.D., Xin, H., and Yu, P. 2013. Investigating the molecular structural features of hulless barley (*Hordeum vulgare* L.) in relation to metabolic characteristics using synchrotron-based Fourier Transform Infrared Microspectroscopy. J. Agric. Food Chem. **61**: 11250–11260. doi:10.1021/jf403196z. PMID:24156528.

Yu, P. 2004. Application of advanced synchrotron radiation-based Fourier transform infrared (SR-FTIR) microspectroscopy to animal nutrition and feed science: a novel approach. Br. J. Nutr. **92**: 869–885. doi:10.1079/BJN20041298. PMID:15613249.

Yu, P. 2005*a*. Multi-component peak modeling of protein secondary structures: comparison of Gaussian with Lorentzian analytical methods for plant feed and seed molecular biology and chemistry research. Appl. Spectrosc. **59**: 1372–1380. doi:10.1366/000370205774783151. PMID:16316515.

Yu, P. 2005*b*. Molecular chemistry imaging to reveal structural features of various plant feed tissues. J. Struct. Biol. **150**: 81–89. doi:10.1016/j.jsb.2005.01.005. PMID:15797732.

Yu, P. 2005*c*. Protein secondary structures (α-helix and β-sheet) at a cellular level and protein fractions in relation to rumen degradation behaviours of protein: a new approach. Br. J. Nutr. **94**: 655–665. doi:10.1079/BJN20051532. PMID:16277766.

Yu, P., Theodoridou, K., Xin, H., Huang, P.-Y., Lee, Y.-C., and Woods, B.R. 2013. Synchrotron-based microspectroscopic study on the effects of heat treatments on cotyledon tissues in yellow-type canola (*Brassica*) seeds. J. Agric. Food Chem. **61**: 7234–7241. doi:10.1021/jf4012517. PMID:23805781.

Zhao, F.J., Moore, K.L., Lombi, E., and Zhu, Y.G. 2014. Imaging element distribution and speciation in plant cells. Trends Plant Sci. **19**: 183–192. doi:10.1016/j.tplants.2013.12.001. PMID:24394523.

Zhao, Q., and Dixon, R.A. 2014. Altering the cell wall and its impact on plant disease: from forage to bioenergy. Annu. Rev. Phytopathol. **52**: 69–91. doi:10.1146/annurev-phyto-082712-102237.